Investigations of Ion Channel Structure-Function Relationships Using Molecular Modeling and Experimental Biochemistry

Thesis by

Donald Eugene Elmore, Jr.

In Partial Fulfillment of the

Requirements for the Degree of

Doctor of Philosophy

California Institute of Technology

Pasadena, California

2004

(Defended April 22, 2004)

Chapter 3: Computational and Experimental Investigation of the C-terminal Region of *M. tuberculosis* MscL

Background

Although cross-linking data in the previous chapter supported the overall crystal structure conformation of Tb-MscL, there are still some ambiguities in the structure. For example, the crystal structure revealed Tb-MscL to be a homopentamer with an □-helical bundle formed by the intracellular C-terminal regions of each subunit (Fig. 3.1). This region has several acidic residues (Asp and Glu) which would be expected to repel one another electrostatically in a bundled structure at physiological pH. However, the crystallization protocol that succeeded in producing acceptable crystals involved a relatively low pH (3.6-3.8) (Chang et al., 1998; Spencer et al., 1999), which would protonate Asp and Glu, potentially reducing their repulsion and stabilizing the □-helical bundle structure. It is thus interesting to consider the extent to which charge neutralization resulting from low pH may have influenced this interesting structural element.

This chapter discusses both computational and experimental work addressing the effect of these charged residues on the conformation of the C-terminal region of MscL. The computational simulations suggest that the observed C-terminal helical bundle conformation may have resulted from the low pH crystallization conditions. In addition, they predict specific mutations that would promote the helix bundle conformation. The effect of these and other mutations on the structural stability of the channel was then tested experimentally using thermal melts monitored by circular dichroism (CD).

Figure 3.1: (*A*) Tb-MscL crystal structure, highlighting the C-terminal helical bundle. Acidic and basic residues in the region are shown in red and blue CPK, respectively. (*B*) Simulation system for MD simulations of the Tb-MscL C-terminal region. The channel is shown as white ribbon with water as blue wireframe and Na^+ and Cl^- ions in green and yellow CPK.

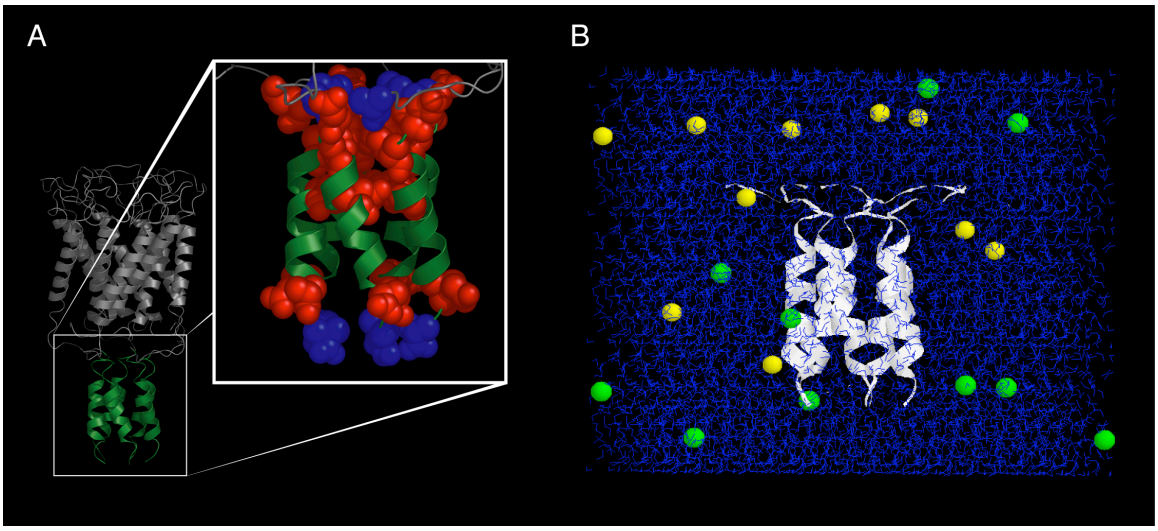

Methods for Computational Modeling of the C-terminal Region

Simulations of the C-terminal region used residues Tyr 94-Arg 118 from all five subunits of the Chang et al. (1998) crystal structure (1MSL) as a starting conformation. Uncharged N- and C-termini (-NH_2 and -COOH) were used, as neither end is a real protein terminus, and the additional charges could cause spurious interactions. Two simulations were performed, which we will refer to as pH 7 and low pH. For the pH 7 simulation, all ionizable residues (Asp, Glu, Lys, and Arg; no His are involved) in the protein were charged. Neutral forms of Asp and Glu were used in the low pH simulation. Additional simulations were performed with various Glu/Gln and Asp/Asn mutations. These were made to the original crystal structure by changing the second acidic O atom

of a residue to an amide N in all five subunits. All remaining ionizable residues were charged in these mutant simulations. These protein structures were then solvated by a box of SPC waters extending 1 nm from the protein in the X, Y, and Z directions. Ions were added randomly to these boxes: 10 Na^+ and 10 Cl^- ions for pH 7, 20 Cl^- ions for low pH, 7 Na^+ and 12 Cl^- for single mutations and 5 Na^+ and 15 Cl^- for the double mutant. These ions were added both to neutralize the charge in the low pH box and to maintain an approximately equal ionic strength between the simulations. The simulations included a total of about 27000 atoms, and after equilibration the system boxes were approximately 6.8 nm x 6.8 nm x 6 nm.

These structures were minimized for 50 steps of steepest descents minimization to reduce close contacts. Minimization was followed by a MD simulation which heated the system to 310 K over 20 ps; after heating all simulations were performed at 310 K. This and all subsequent MD runs on these systems included restraints on the Cα atoms of the two N-terminal residues of each subunit to represent conformational restrictions imposed by the overall assembly of the channel. All MD runs used a timestep of 2 fs along with the LINCS routine to constrain bond lengths (Hess et al., 1997) and SETTLE to constrain water geometries (Miyamoto and Kollman, 1992). Lennard-Jones and short-range Coulombic interactions were cutoff at 1.0 nm, and long-range electrostatics were calculated with particle-mesh Ewald methods, using Fourier grid spacing of 0.10 nm and cubic interpolation. The NPT ensemble with periodic boundary conditions was employed for all runs with isotropic pressure coupling to 1 bar and a coupling constant (τ_p) of 1.0 ps (Berendsen et al., 1984). All minimizations and MD simulations were performed using GROMACS 2.0 (Berendsen et al., 1995) with standard GROMACS parameters.

Analyses of the trajectories were primarily performed with tools included in the GROMACS suite (Berendsen et al., 1995). Properties were averaged over the last 1000 ps of trajectories. Additionally, the DSSP program was used to determine secondary structure (Kabsch and Sander, 1983).

The Effect of pH on the C-terminal Helix Bundle in MD Simulations

The pH 7 and low pH trajectories were noticeably different from one another. The pH 7 simulation had a much larger Cα RMS deviation from the crystal structure than the one at lower pH, showing the overall conformation was more preserved in the lower pH simulation (Fig. 3.2*A*). Although these 1.5 ns simulations are not particularly lengthy, computed RMS fluctuations may give qualitative insight into the relative stabilities of the trajectories, and the low pH case did exhibit consistently lower Cα RMS fluctuations for the majority of the structure (Fig. 3.2*B*).

In addition, the α-helical secondary structure is much better preserved in the low pH simulation, while many of the α-helices have been largely eroded by the end of the pH 7 trajectory. This can be seen by DSSP analysis per residue over the trajectories (Fig. 3.3), and from the final structures in Fig. 3.4. In the pH 7 simulation, the acidic groups appear to have repulsed each other, leading to the overall deformation of the crystal structure conformation. Such a repulsion is not seen with the neutralized residues in the low pH case, as can be seen by multiple Glu 104 and Asp 108 side chains pointing towards one another in the final structure.

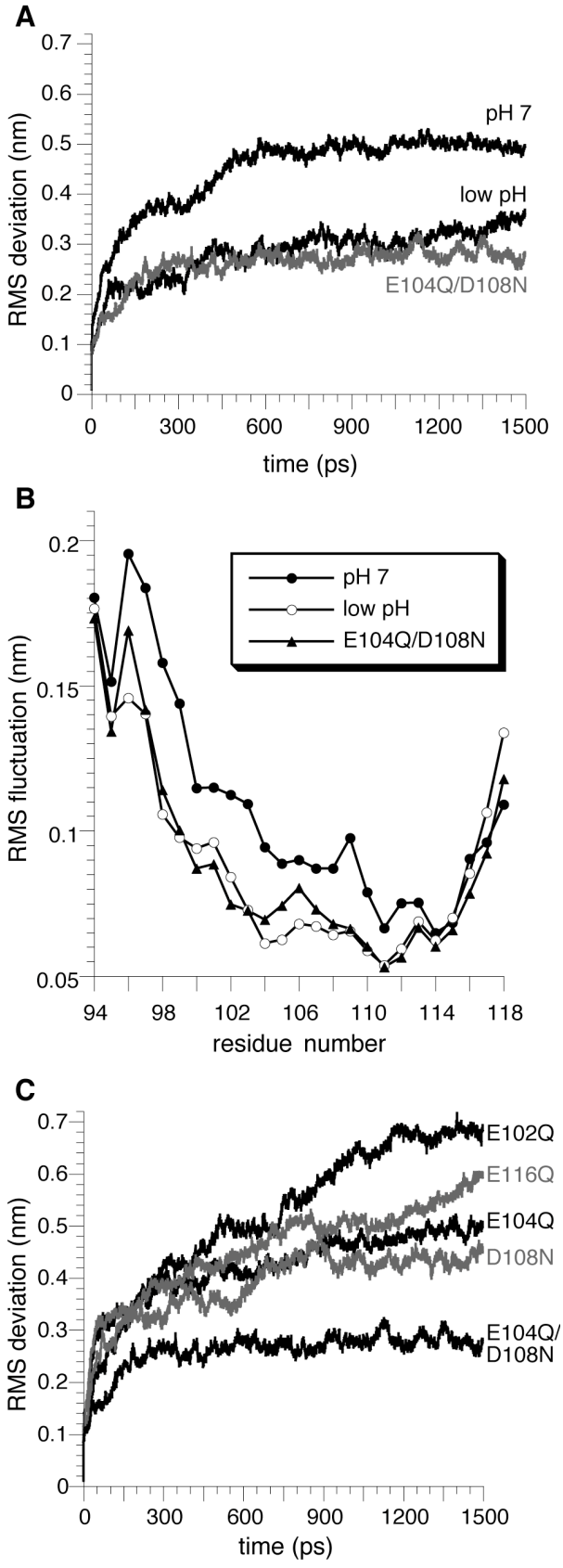

Figure 3.2: (*A*) RMS deviation of Cα from the crystal structure for the pH 7, low pH, and E104Q/D108N C-terminal region simulations, calculated for each frame after fitting the trajectory Cα to the crystal structure. (*B*) RMS fluctuation of Cα around an average structure for C-terminal region simulations plotted per residue. The computed RMS fluctuation is averaged over the five chains. Single mutant fluctuations are omitted for clarity. Values for the E102Q and E116Q simulations were generally in the range of the pH 7 simulation, while E104Q and D108N showed lower fluctuations than pH 7 from the N-terminus to the mutation sites. (*C*) RMS deviation of Cα from the crystal structure for amide mutation trajectories, calculated as described in *A*.

Figure 3.3: Analysis of secondary structure for the C-terminal region simulations performed with the DSSP method for the pH 7, low pH, and E104Q/D108N simulations. Black portions represent residues that are α-helical at a given point in the trajectories. Results for one representative "subunit" from each trajectory is shown.

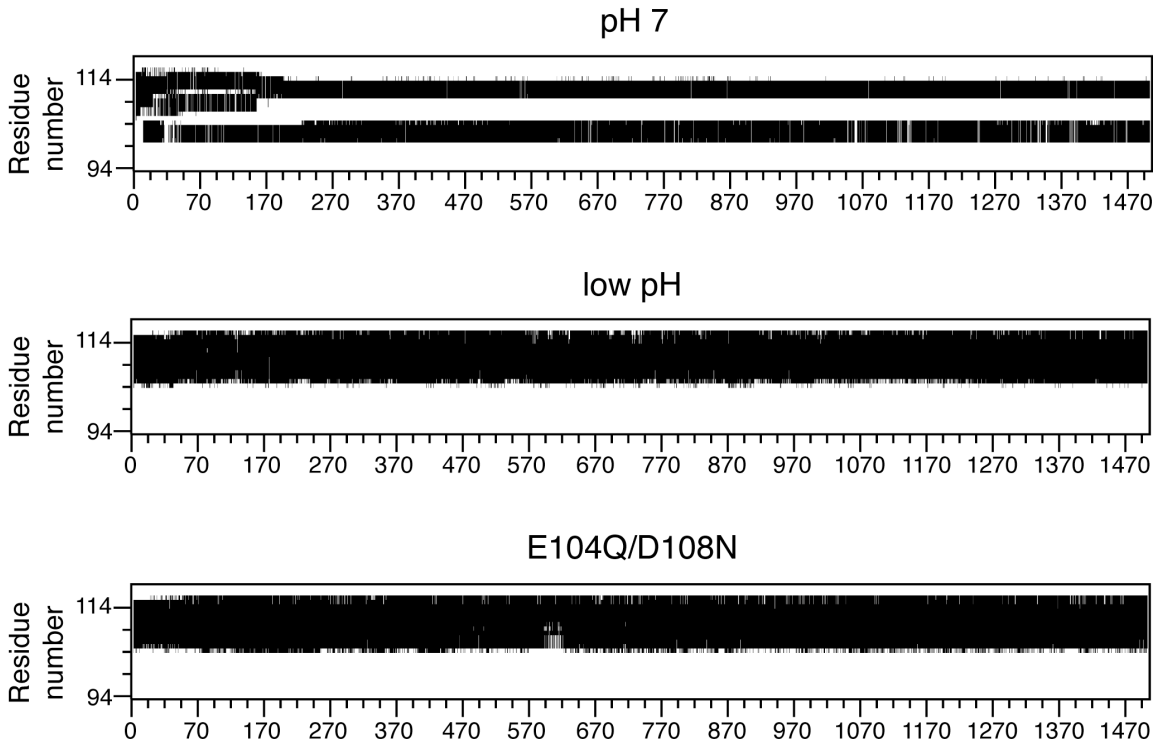

The present simulations suggest that the intracellular helix bundle of Tb-MscL was stabilized by the low pH of the crystallization medium, a possibility suggested by Rees and co-workers (Chang et al., 1998; Spencer et al., 1999). However, such a helix bundle might still be physiologically relevant, perhaps stabilized by binding to metal ions or polyamines. In a case where many acidic residues are constrained into close proximity they could exhibit a shifted pKa, causing some or all to remain protonated under physiological conditions. In fact, experimental data discussed below implies that such pKa shifts might occur to some, but likely not all, residues in the region. The region might also be stabilized by protein-lipid interactions, as discussed in Chapter 5.

Figure 3.4: Ribbon diagrams of the final frames (1500 ps) of the pH 7, low pH and E104Q/D108N C-terminal region simulations. The analogous region of the crystal structure is also shown. In all structures, the acidic residues (or their mutated amide counterparts) are shown in CPK.

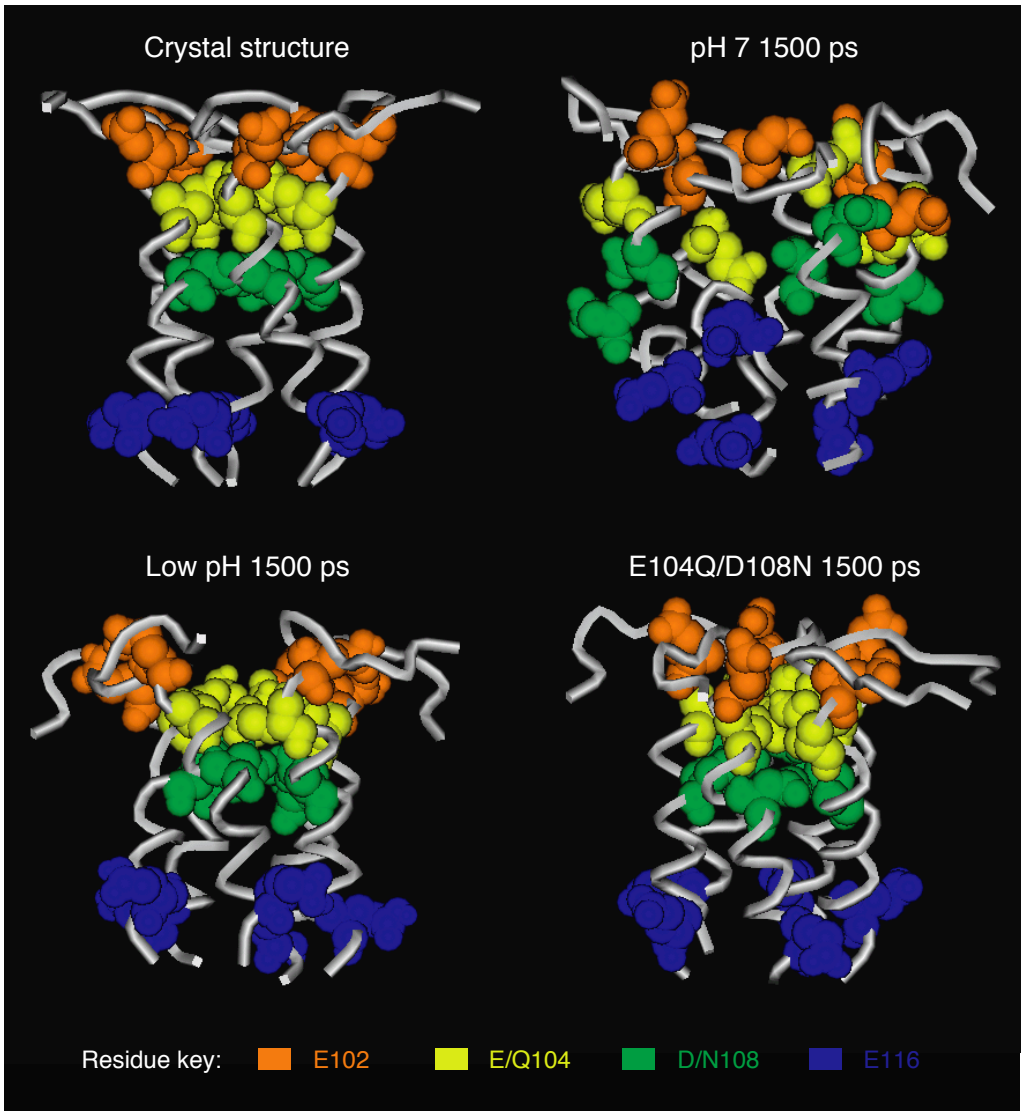

Additionally, ambiguity in the physiological conformation of the C-terminal helical bundle does not imply any uncertainty in the overall pentameric channel conformation observed in the crystal structure. In fact, the crystal structure

conformation, particularly that of the TM helices, was well preserved in simulations of the channel described in Chapters 4 and 5 with ionized side chain protonation states.

The Effect of Mutations to the C-terminal Helix Bundle in Computations

In order to determine if diminishing electrostatic repulsions in the C-terminal region could stabilize the helix bundle at pH 7, we have selectively converted acidic residues (Glu and Asp) to their amide counterparts (Gln and Asn). These Asn and Gln side chains would be extremely similar sterically and electrostatically to protonated Asp and Glu. Thus, trajectories for the C-terminal region with single mutations of all four acidic residues (E102Q, E104Q, D108N, and E116Q) were computed. For the most part these single mutations led to trajectories similar to that of the wild-type pH 7 simulation, as measured by Cα RMS deviation from the crystal structure (Fig. 8.2*C*), Cα RMS fluctuation, and secondary structure conservation by DSSP (data not shown). However, visual inspection of the E104Q and D108N trajectories did indicate that these mutations did somewhat conserve the helical bundle, albeit far less than seen in the low pH situation. As well, there was some reduction in Cα RMS fluctuation from the N-terminus to the mutation site in each of those simulations (data not shown).

These hints of partial stabilization with the E104Q and D108N mutations led us to perform an additional trajectory with a E104Q/D108N double mutant. As can be seen by Cα RMS deviation (Fig. 3.2*C*), Cα RMS fluctuation (Fig. 3.2*B*), and DSSP secondary structure determination (Fig. 3.3), the combined effect of the two mutations led to a trajectory equivalent to that of the low pH simulation. The final structure from the

E104Q/D108N simulation is also strikingly similar to that from the low pH simulation (Fig. 3.4).

Thus, an E104Q/D108N double mutation may have similar effects to low pH conditions on the structure of the Tb-MscL C-terminal helix bundle. As well, mutations of the other charged residues in the region may alter structural stability. Therefore, we attempted to experimentally investigate the effects of this and other mutations on MscL structural stability.

Experimental Production of MscL with C-terminal Mutations

The Tb-MscL channel was encoded in the pET 19b vector, and protein expression was performed in MscL null *E. coli* BL21 cells (Chang et al., 1998; Maurer et al., 2000). The pET 19b vector provides ampicillin resistance and IPTG control over protein expression. Site-directed mutagenesis of the channel was performed using the QuikChange protocol (Stratagene, La Jolla, CA) in order to make mutations to charged residues throughout the C-terminal region: K100Q, E102C, E104Q, D108N, E116Q, E116D, R118Q, D119N, D127N, D142N, and E149Q. As well, a few additional mutations were made to non-charged residues: L113I, T115A, L117I, and L121I. All mutants were verified by sequencing and enzymatic digestion.

For the production of channel protein, frozen permastocks of Tb-MscL or Tb-MscL mutations were used to inoculate 25 mL of LB media with 100 μg/mL ampicillin. The cultures were grown overnight at 37˚C with shaking, and were then used to inoculate 500 mL of TB media with ampicillin. The resulting TB cultures were grown to mid-log phase and then induced with 1 mM IPTG. After induction, the cultures were grown for

an additional 2 hours at 37 ˚C or in some cases for 3 hours at 30 ˚C. Bacteria were then pelleted, and resuspended in 50 mM Tris / 75 mM NaCl / 1% β-dodecyl maltoside (DDM) at pH 7.5 (10 mL) with Complete protease inhibitor cocktail (Roche, Indianapolis, IN). The suspensions were then probe sonicated (4 x 30 Sec.) and incubated with shaking for 1 hour at 37˚C. Following incubation, the suspensions were pelleted at 45,000 x g for 45 minutes and the resulting supernate was passed through a 0.2 μm filter. The L117I and R118Q mutant proteins showed extensive proteolysis of the carboxyl terminal tail that was not observed for other proteins. Therefore, they could not be produced in sufficient quantities for CD thermal melts.

All chromatography steps for protein purification were carried out on a Vision Workstation (Applied Biosystems, Foster City, CA). The clarified supernate was subjected to two-dimensional chromatography, using a POROS metal chelate affinity column (Applied Biosystems, Foster City, CA) charged with cobalt chloride in the first dimension and a POROS HQ anion exchange column (Applied Biosystems, Foster City, CA) in the second dimension. Elution from the metal chelate column was achieved using an imidazole gradient (0.25 mM-1 M at pH 7.5) with 0.05% DDM and elution from the HQ column was achieved using a sodium chloride gradient (0 mM-1 M) in the presense of 10 mM Tris at pH 7.5 and 0.05% DDM. Buffer exchange and desalting were then performed using a HiPrep 26/10 desalting column (Amersham Pharmacia Biotech, Piscataway, NJ) charged with 1 mM phosphate buffer and 0.05% DDM at pH 7.2.

Characterization of MscL Mutants with Thermal Melts

Thermal denaturation was used to investigate if the Tb-MscL C-terminal mutants caused structural perturbations in addition to inducing functional changes. All thermal denaturation was performed using an Aviv 62 DS circular dichroism spectrophotometer (Aviv Instruments, Lakewood, NJ). Purified Tb-MscL protein samples were diluted to approximately identical concentrations in 1 mM phosphate buffer (pH 7.2) for thermal denaturation. Circular dichroism scans (260-195 nm) showed equivalent helical propensities between samples. The denaturation consisted of heating from 25 °C to 95 °C, stepping every 2.5 °C, and allowing the sample to equilibrate at each temperature for 5 min. After equilibration, the ellipticity of samples at 220 nm was measured, averaging the signal over 30 s.

The denaturation curve for wild-type Tb-MscL shows a single melting transition (T_m) around 60 °C (Fig. 3.6). A reduction of 35% in the CD signal is observed between 25 °C and 95 °C. Thus, significant helicity remains in the sample even after the observed transition, which most likely corresponds to the transmembrane domains. After melting, Tb-MscL regains the majority (>90%) of its original elipticity upon returning to 25 °C.

The Tb-MscL C-terminal mutant denaturation curves were qualitatively similar to that of wild type. However, changes in T_m arose for some mutants. In particular, a major shift in T_m to a lower temperature was noted for E116D. Interestingly, an analogous shift was *not* noted for the E116Q mutation. In other words, shortening the carboxylic acid side chain by one methylene unit resulted in a dramatic change in structural stability, while neutralizing the charge on the residue had no effect on stability. Thus, it seems likely that this residue plays an important steric role in the C-terminal structure.

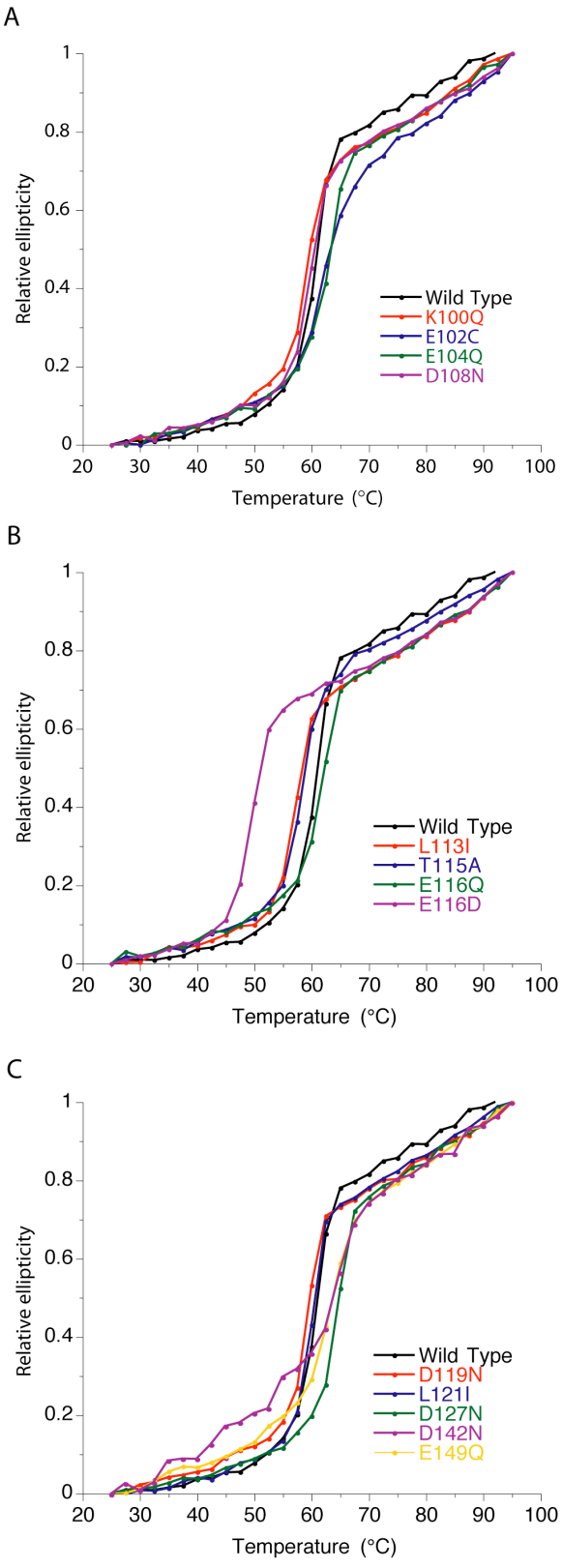

Figure 3.6: Circular dichroism thermal denaturation curves for wild-type Tb-MscL and a series of single-site C-terminal mutations. A) Mutations in the upper portion of the crystal structure C-terminal region. B) Mutations in the lower portion of the crystal structure C-terminal region. C) Mutations to residues not in the crystal structure.

Additionally, since there is no apparent effect of mutating the glutamic acid at position 116 to the corresponding amide, it seems that residue 116 either has a shifted pKa and is neutral at pH 7.2 or that the negative charge is not important at this position.

Other mutations showed an *increased* stability upon charge neutralization. The T_m shifted to a moderately higher temperature for D127N, and to slightly higher temperatures for E102C, E104Q, D142N, and E149Q. These results agree generally with the computational prediction that neutralizing negatively charged residues would lead to an overall stabilization in the region. In addition, these residues likely do *not* experience a significant pKa shift in the assembled channel structure, since neutralizing them has a distinct effect on channel stability.

Two mutations to uncharged residues, L113I and T115A, also showed an effect on structural stability, slightly decreasing T_m. L113I lies on the helical face discussed below that might line the inside of the helical bundle in the physiological structure. Thus, this site may be sensitive to mutation because of important steric contacts made by the leucine side chain. However, the effect observed for T115A is difficult to explain without further experimentation.

Developing Structural Models of the MscL C-terminal Region

Previous modeling has proposed a generally helical structure for the carboxyl terminus of many MscL homologues, including coiled coil regions for some species (Hamill and Martinac, 2001; Sukharev et al., 2001). As well, TASP studies have implied that the assembled Tb-MscL carboxyl terminal region is highly helical (Kochendoerfer et al., 2002). The experimental structural stability data in this chapter are consistent with

the C-terminal region having an extended α-helical secondary structure, since when the thermal melt data is mapped on a helical wheel, all of the mutations that led to altered structural stability reside on one face of the helix, except for E104Q and T115A (Fig. 3.7). This type of extended C-terminal helix structure would be reminiscent of the KcsA C-terminal structure determined by EPR (Cortes et al., 2001).

It is interesting to note that a stabilizing effect was not observed for D108N, although computations implied that charge neutralization at that site would significantly affect the stability of the region. This could mean that the D108 are in close proximity and undergo a pKa shift in the assembled structure. If this is true, then a mutation that decreases the steric bulk at site 108, such as D108A, might affect structural stability, analogous to how E116D showed a significant shift in T_m. However, it seems more likely that under physiological conditions that the C-terminal helical bundle might rearrange slightly, such that the helical face containing the mutants that alter stability line the inside of the bundle instead of the face containing E104 and D108, which lines the inside in the crystal structure. This would be consistent with E116 forming an important steric contact between helices and with the lack of effect seen for the D119N mutant, which lies on the same face as residues 104 and 108. A similar rearrangement of the helical bundle was also proposed by Sukharev and co-workers, although their proposed rotation is slightly different, placing the helical face between L114 and L120 at the inside of the bundle (Anishkin et al., 2003).

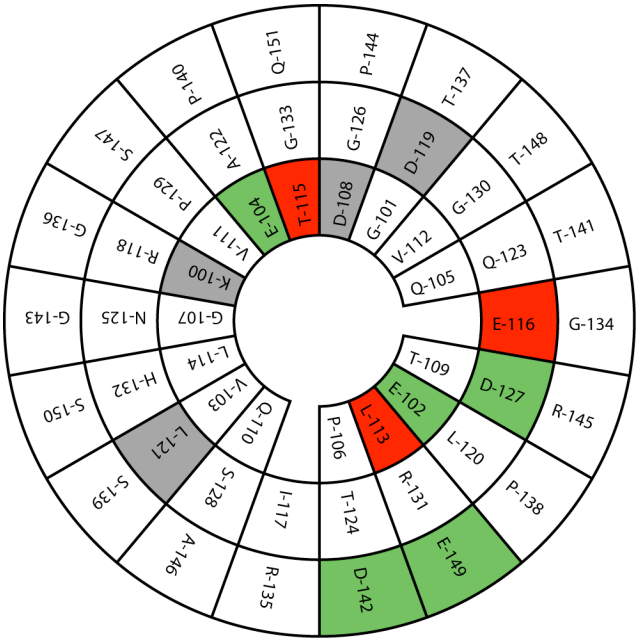

Figure 3.7: Helical wheel showing observed shifts in thermal stability for mutations in the carboxyl terminal region of Tb-MscL. Gray coloring indicates no shift, green indicates a shift to a higher T_m (a stabilizing mutant), and red indicates a shift to a lower T_m (a destabilizing mutant).

Although the helical rotations described above explain the stability data in a fairly straightforward manner, other structural models could be proposed. For example, it is also possible that instead of forming one long extended helix that the region contains a bend causing the most distal region to interact with the region visible in the crystal structure. A cartoon of this sort of structure is shown in Fig. 3.8. The high density of proline and glycine residues between sites 116 and 142 (32% of residues) could allow for this bend to occur, allowing interactions between regions separated in sequence space. Future work on the structural and functional affects of these and other mutations in the region may be able to support this model, the extended helix model, or another structural motif for the region.

Figure 3.8: A cartoon depicting one possible conformation of a Tb-MscL single subunit with a "bend" in the C-terminal region. The residues in the crystal structure are shown in blue and the C-terminus, which could not be resolved in the crystal structure, is shown in red.

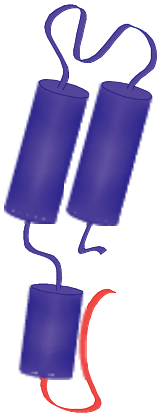

Summary

Calculations involving only the intracellular C-terminal region of Tb-MscL were used to investigate the effect of different side chain protonation states on the stability of the C-terminal helix bundle. Conservation of the crystal structure conformation was greatly increased by neutralizing the acidic Asp and Glu residues in this region, which would occur under low pH conditions such as those used for crystallization. This increased stability at low pH may have aided in the crystallization of the channel. Several computational mutations to this region were made in attempts to replicate the effects of low pH under physiological pH conditions. Although single mutations did not have much effect on the region, an E104Q/D108N double mutant afforded a helix bundle conformation equivalent to that of the low pH model.

One limitation of these simulations is that they do not include any interactions that might occur between the C-terminus and the lipid. If lipid interactions play a significant role in stabilizing—or destabilizing—the C-terminal region, then considering these interactions more explicitly in other simulations could lead to more detailed insights

into the structure of this region. In fact, subsequent simulations of the full channel structure embedded in the lipid membrane described in Chapter 5 have pointed to a significant role for lipid stabilization in this region.

Although the experimental data has begun to give us some insight into the effect of mutations in the Tb-MscL C-terminus on the stability of the channel, many questions remain. Most importantly, it is still unknown whether or not most of these mutations affect channel function. One of the mutants, E104Q, has been electrophysiologically characterized as a gain-of-function mutation, requiring much less membrane tension to open than wild-type Tb-MscL (Shapovalov et al., 2003). This mutation was also observed to stabilize the structure of the channel in thermal denaturation studies. It will be interesting to investigate whether similar physiological effects will be observed for the other mutations that altered structural stability. In addition, functional characterization will give interesting insight into the intriguing pair of mutations to E116.

References

Anishkin, A., V. Gendel, N. A. Sharifi, C. S. Chiang, L. Shirinian, H. R. Guy, and S. Sukharev. 2003. On the conformation of the COOH-terminal domain of the large mechanosensitive channel MscL. *J. Gen. Physiol.* 121:227-44.

Berendsen, H. J. C., J. P. M. Postma, W. F. van Gunsteren, A. DiNola, and J. R. Haak. 1984. Molecular dynamics with coupling to an external bath. *J. Chem. Phys.* 81:3684-3690.

Berendsen, H. J. C., D. van der Spoel, and R. van Drunen. 1995. GROMACS: A message-passing parallel molecular dynamics implementation. *Comp. Phys. Comm.* 91:43-56.

Chang, G., R. H. Spencer, A. T. Lee, M. T. Barclay, and D. C. Rees. 1998. Structure of the MscL homolog from *Mycobacterium tuberculosis*: a gated mechanosensitive ion channel. *Science* 282:2220-6.

Cortes, D. M., L. G. Cuello, and E. Perozo. 2001. Molecular architecture of full-length KcsA: role of cytoplasmic domains in ion permeation and activation gating. *J Gen Physiol* 117:165-80.

Hamill, O. P., and B. Martinac. 2001. Molecular basis of mechanotransduction in living cells. *Physiological Reviews* 81:685-740.

Hess, B., H. Bekker, H. J. C. Berendsen, and J. G. E. M. Fraaije. 1997. LINCS: A linear constraint solver for molecular simulations. *J. Comp. Chem.* 18:1463-1472.

Kabsch, W., and C. Sander. 1983. Dictionary of protein secondary structure—Pattern-recognition of hydrogen-bonded and geometrical features. *Biopolymers* 22:2577-2637.

Kochendoerfer, G. G., J. M. Tack, and S. Cressman. 2002. Total chemical synthesis of a 27 kDa TASP protein derived from the MscL ion channel of *M. tuberculosis* by ketoxime-forming ligation. *Bioconjugate Chemistry* 13:474-480.

Maurer, J. A., D. E. Elmore, H. A. Lester, and D. A. Dougherty. 2000. Comparing and contrasting *Escherichia coli* and *Mycobacterium tuberculosis* mechanosensitive channels (MscL) - New gain of function mutations in the loop region. *Journal of Biological Chemistry* 275:22238-22244.

Miyamoto, S., and P. A. Kollman. 1992. SETTLE: An analytical version of the SHAKE and RATTLE algorithms for rigid water models. *J. Comp. Chem.* 13:952-962.

Shapovalov, G., R. Bass, D. C. Rees, and H. A. Lester. 2003. Open-state disulfide cross-linking between *Mycobacterium tuberculosis* mechanosensitive channel subunits. *Biophys J* 84:2357-65.

Spencer, R. H., G. Chang, and D. C. Rees. 1999. "Feeling the pressure": Structural insights into a gated mechanosensitive channel. *Curr. Opin. Struct. Biol.* 9:448-454.

Sukharev, S., S. R. Durell, and H. R. Guy. 2001. Structural models of the MscL gating mechanism. *Biophys. J.* 81:917-936.